Ammonia in the summertime Arctic marine boundary layer: Sources, Sinks and Implications

G. R. Wentworth[1], J. G. Murphy[1], B. Croft[2], R. V. Martin[2], J. R. Pierce[3,2], J.-S. Côté[4], I. Courchesne[4], J.-É. Tremblay[4], J. Gagnon[4], J. L. Thomas[5], S. Sharma[6], D. Toom-Sauntry[6], A. Chivulescu[6], M. Levasseur[4], and J. P. D. Abbatt[1]

[1]{Department of Chemistry, University of Toronto, 80 St. George Street, M5S 3H6, Toronto, Canada}

[2]{Department of Physics and Atmospheric Science, Dalhousie University, 6310 Coburg Road, B3H 4R2, Halifax, Canada}

[3]{Department of Atmospheric Science, Colorado State University, 3915 W. Laporte Ave., 80523, Fort Collins, USA}

[4]{Department of Biology, Université Laval, 1045 avenue de la Médicine, G1V 0A6, Québec City, Canada}

[5]{Sorbonne Universités, UPMC Univ. Paris 06; Université Versailles St-Quentin; CNRS/INSU, LATMOS-IPSL, Paris, France}

[6]{Science and Technology Branch, Environment Canada, 4905 Dufferin Street, M3H 5T4, Toronto, Canada}

Correspondence to: J. G. Murphy (jmurphy@chem.utoronto.ca)

Abstract

Continuous hourly measurements of gas-phase ammonia ($NH_{3(g)}$) were taken from 13 July to 7 August 2014 on a research cruise throughout Baffin Bay and the eastern Canadian Arctic Archipelago. Concentrations ranged from 30-650 ng m^{-3} (40-870 pptv) with the highest values recorded in Lancaster Sound (74°13' N, 84°00' W). Simultaneous measurements of total ammonium ($[NH_x]$), pH and temperature in the ocean and in melt ponds were used to compute the compensation point (χ), which is the ambient $NH_{3(g)}$ concentration at which surface-air fluxes change direction. Ambient $NH_{3(g)}$ was usually several orders of magnitude larger than

both χ_{ocean} and χ_{MP} (<0.4-10 ng m^3) indicating these surface pools are net sinks of NH_3. Flux calculations estimate average net downward fluxes of 1.4 and 1.1 ng m^{-2} s^{-1} for the open ocean and melt ponds, respectively. Sufficient $NH_{3(g)}$ was present to neutralize non-sea salt sulphate (nss-SO_4^{2-}) in the boundary layer during most of the study. This finding was corroborated with a historical dataset of $PM_{2.5}$ composition from Alert, NU (82°30' N, 62°20' W) wherein the median ratio of NH_4^+/nss-SO_4^{2-} equivalents was greater than 0.75 in June, July and August. The GEOS-Chem chemical transport model was employed to examine the impact of $NH_{3(g)}$ emissions from seabird guano on boundary-layer composition and nss-SO_4^{2-} neutralization. A GEOS-Chem simulation without seabird emissions underestimated boundary layer $NH_{3(g)}$ by several orders of magnitude and yielded highly acidic aerosol. A simulation that included seabird NH_3 emissions was in better agreement with observations for both $NH_{3(g)}$ concentrations and nss-SO_4^{2-} neutralization. This is strong evidence that seabird colonies are significant sources of NH_3 in the summertime Arctic, and are ubiquitous enough to impact atmospheric composition across the entire Baffin Bay region. Large wildfires in the Northwest Territories were likely an important source of NH_3, but their influence was probably limited to the Central Canadian Arctic. Implications of seabird-derived N-deposition to terrestrial and aquatic ecosystems are also discussed.

1 Introduction

Ammonia ($NH_{3(g)}$) is the dominant alkaline gas in the atmosphere and is an important component of the global nitrogen cycle. Its transport and deposition can have harmful effects for N-sensitive ecosystems such as eutrophication, loss of biodiversity and soil acidification (Krupa, 2003). The presence of $NH_{3(g)}$ can impact climate by increasing rates of new particle formation via stabilization of sulphuric acid clusters (Kirkby et al., 2011). Gas-phase NH_3 is also able to partition to acidic fine particulate matter ($PM_{2.5}$) to form particulate-phase ammonium ($NH_4^+{}_{(p)}$), which alters various aerosol properties, such as scattering efficiency (Martin et al., 2004), hygroscopicity (Petters and Kreidenweis, 2007), ice nucleating ability (Abbatt et al., 2006) and heterogeneous chemistry occurring on surfaces (Fickert et al., 1999).

As a result, the accurate quantification of the magnitude and location of $NH_{3(g)}$ sources is important for chemical transport models (CTMs). The major anthropogenic source is agriculture (fertilization and animal husbandry) with biomass burning, transport and industry being minor contributors (Reis et al., 2009). Natural sources include soils, vegetation, oceans

and animal excreta (Sutton et al., 2013). Estimates for the annual global emissions of $NH_{3(g)}$ range from 35-54 Tg N yr^{-1}; however, large uncertainties exist for these values due to the area-wide nature (emissions spread over a large spatial extent) and poor characterization of many sources. In remote marine environments, the ocean is thought to be the dominant source of $NH_{3(g)}$ to the marine boundary layer and delivers an estimated 6-8 Tg N yr^{-1} to the atmosphere globally (Sutton et al., 2013). The dominant sources of oceanic NH_x ($\equiv NH_3 + NH_4^+$) include remineralisation of organic matter by bacteria and phytoplankton excretion (Carpenter et al., 2012). However, NH_x is an extremely labile nutrient for microbes such that assimilation by phytoplankton and bacteria prevents significant accumulation in surface waters. Nonetheless, there exists a pool of dissolved ammonia ($NH_{3(sw)}$) available for exchange with the atmosphere.

In order to compute sea-air NH_3 fluxes, simultaneous measurements of both atmospheric $NH_{3(g)}$ and oceanic NH_x are required. These measurements are extremely challenging due to low ambient concentrations and complications arising from making ship-based measurements (e.g. proximity to human activity can cause artefacts). As a result, to our knowledge only six previous studies have simultaneously quantified both [$NH_{3(g)}$] and oceanic [NH_x], leading to extremely large uncertainties for both the direction and magnitude of global sea-air NH_3 fluxes (Asman et al., 1994; Geernaert et al., 1998; Gibb et al., 1999; Johnson et al., 2008; Quinn et al., 1988, 1990). Johnson et al. (2008) provided the most recent dataset and summarized the previous studies to show that the open ocean can be both a net source and a net sink of $NH_{3(g)}$, with sea surface temperature (SST) being a key determinant for the direction of flux. Colder SST reduces the emission potential due to increased solubility of NH_3 (because of both reduced $NH_{3(aq)}$ volatility and increased partitioning of $NH_{3(aq)}$ to $NH_4^+{}_{(aq)}$); hence, at higher latitudes the open ocean is more likely to act as a net sink (Johnson et al., 2008). Of the six previous studies, only Johnson et al. (2008) quantified NH_3 fluxes above the Arctic Circle (66°33' N) during a summer time study in the Norwegian Sea. Therefore additional measurements of sea-air NH_3 fluxes in the High Arctic are invaluable for improving constraints on oceanic NH_3 emissions.

During the summertime, freshwater melt ponds are a ubiquitous feature on top of melting Arctic sea ice and can comprise up to 80% of the sea ice surface (Lüthje et al., 2006). These melt ponds form from melting sea ice and are anywhere from a few cm to over 1 m deep. They are chemically distinct from the bulk ocean owing to their low salinity and physical separation from the ocean mixed layer by sea ice or stratification. To our knowledge, no studies to date have

attempted to quantify melt pond-air $NH_{3(g)}$ fluxes despite the abundant presence of melt ponds in the summertime Arctic.

Quantifying sea-air and melt pond-air NH_3 exchange in the Arctic will help elucidate the role these processes play as either sources or sinks in the Arctic nitrogen cycle. Many terrestrial Arctic ecosystems are N-limited and highly sensitive to perturbations in N-input (Shaver and Chapin III, 1980), thus Arctic soils and vegetation are unlikely to represent important sources of atmospheric ammonia. Major sources at lower latitudes include agriculture, vegetation, transport and industry (Reis et al., 2009; Sutton et al., 2013) but these are expected to contribute minimally north of the Arctic Circle. Since the lifetime of $NH_{3(g)}$ is typically less than 24 h, long-range transport from lower latitudes is likely not important (Lefer et al., 1999). Substantial NH_3 emissions have been measured from both seabird guano (Blackall et al., 2007) and seal excreta (Theobald et al., 2006) so large colonies may be relevant point sources throughout the Arctic region. Biomass burning can also inject significant quantities of NH_3 into the free troposphere and/or boundary layer (Bouwman et al., 1997). Although vegetation in the high Arctic is sparse, there can be large wildfires in boreal regions, and emissions may be transported poleward. The potential for the ocean and melt ponds to act as sources to the atmosphere will depend on the relative importance of sources and sinks within the atmosphere and the aqueous systems.

NH_3 emission to the atmosphere can affect the extent of non-sea salt sulphate ($nss\text{-}SO_4^{2-}$) neutralization, which has implications for N-transport (Lefer et al., 1999). Therefore, it is important to also consider the relative abundances of atmospheric NH_x and $nss\text{-}SO_4^{2-}$. The dominant source of the latter in the summertime Arctic is oxidation of dimethylsulphide (DMS) emitted from the Arctic Ocean (Leaitch et al., 2013; Sharma et al., 1999, 2012). Measurements of $PM_{2.5}$ composition in the summertime Arctic marine boundary layer are rare (e.g. Chang et al., 2011; Leck et al., 2001). Previous chemical transport model (CTM) studies with GEOS-Chem predict highly acidic aerosol (i.e. $nss\text{-}SO_4^{2-} >> NH_x$) with negligible amounts of $NH_{3(g)}$ throughout the summertime Arctic boundary layer (Breider et al., 2014).

The region for this study is the eastern Canadian Arctic Archipelago where ship-based atmospheric ($NH_{3(g)}$, $NH_4^+{}_{(p)}$, $SO_4^{2-}{}_{(p)}$) and oceanic ([NH_x], pH, SST) measurements were taken over a 4-week period in July and August, 2014. To our knowledge, this study presents the first measurements of $NH_{3(g)}$ in the Canadian Arctic. Motivated by a lack of atmospheric and oceanic

measurements in the region, as well as substantial uncertainties in sea-air and melt pond-air NH_3 fluxes, the specific goals of this study were to:

1) Simultaneously quantify $NH_{3(g)}$ and oceanic/melt pond [NH_x] to infer surface-air NH_3 fluxes
2) Assess the relative abundances of $NH_{3(g)}$, $NH_4^{+}{}_{(p)}$ and $SO_4^{2-}{}_{(p)}$ to determine the extent of $SO_4^{2-}{}_{(p)}$ neutralization
3) Elucidate the major sources and sinks of atmospheric NH_3 throughout the summertime Arctic marine boundary layer
4) Evaluate whether atmospheric NH_x deposition could be an important N-input to aquatic and terrestrial Arctic ecosystems

2 Materials and Methods

2.1 2014 CCGS *Amundsen* Cruise

Measurements were taken aboard the Canadian Coast Guard Ship *Amundsen* between 13 July and 7 August 2014 as part of the Network on Climate and Aerosols: Addressing Key Uncertainties in Remote Canadian Environments (NETCARE). The CCGS *Amundsen* departed from Québec City, Québec on 8 July 2014 and sailed throughout the Eastern Canadian Archipelago heading as far north as 81.47 °N eventually reaching Kugluktuk, Nunavut on 13 August 2014. A detailed map of the ship's route for this leg is shown in Fig. 1 along with the ship's position at the start of selected days. All times are given in co-ordinated universal time (UTC).

2.2 Atmospheric Measurements

Ambient levels of water-soluble ions in $PM_{2.5}$ (NH_4^+, SO_4^{2-}, and NO_3^-) and their precursor gases (NH_3, SO_2, and HNO_3) were measured using the Ambient Ion Monitor-Ion Chromatograph (AIM-IC) system (Model 9000D, URG Corp., Chapel Hill, NC). The AIM-IC is a continuous on-line system which provides simultaneous gas-phase and particle-phase measurements with hourly time resolution. The system has been adapted to locate the gas and particle separation and collection hardware as close as possible to the inlet sampling point (Markovic et al., 2012). Ambient air is pulled through a $PM_{2.5}$ impactor to remove coarse (>2.5 μm in diameter) particles at a flow of 3 L min^{-1}. Air then enters a parallel plate wet denuder where water-soluble gases are dissolved in a 2 mM H_2O_2 solution (to enhance the solubility of SO_2) which is continuously

flowing across the denuder membranes. The remaining $PM_{2.5}$ particles have sufficient inertia to pass through the denuder into a supersaturation chamber where they are collected as an aqueous solution via hygroscopic growth. These components were contained within an aluminum inlet box that was mounted to the hull near the bow of the ship (about 4 m back of the bow). The height of the inlet was 1 m above the deck. Influence from ship-generated sea spray was likely minimal due to the benign nature of the summertime Arctic Ocean, in addition to the $PM_{2.5}$ impactor designed to remove coarse particles. The aqueous solutions collected in the inlet box were pulled down a 22 m sample line through a conduit leading to the IC systems which were housed in a laboratory below deck. Half of each ~10 mL aqueous aliquot (representing 1 hour of sampling) was then separately injected onto both a cation IC and anion IC for quantification of water-soluble ions.

The IC systems (ICS-2000, Dionex Inc., Sunnyvale, CA) were operated using CS17/AS11-HC analytical columns, CG17/AG11-HC guard columns and TCC-ULP1/TAC-ULP1 concentrator columns for improved detection limits. Reagent-free gradient elution schemes and suppressed conductivity were also employed. Aqueous standards of known concentration were prepared via serial dilution of commercially available mixed standards (Dionex Corp., Sunnyvale, CA) containing 6 cations (P/N 040187) and 7 anions (P/N 056933). Manual injection of these standards yielded reasonable ($R^2 > 0.99$) six-point calibration curves.

During the campaign, three zero air overflow experiments were performed to quantify the background signal of each analyte measured during AIM-IC ambient sampling. For each experiment the inlet was overflowed with high purity zero air (AI 0.0 UZ-T, PraxAir, Toronto, ON) at 4.5 L min^{-1} for 18 hours. The average peak area during the final 8 hours of each experiment was used as a background and subtracted from each ambient measurement. Detection limits were calculated by taking 3 times the standard deviation of each analyte peak area during the final 8 hours of each zero air overflow. This value was then converted to either a mixing ratio or mass loading assuming standard temperature and pressure (STP). Detection limits for species of interest during the cruise were 29 ng m^{-3} (NH_3), 17 pptv (SO_2), 8 pptv (HNO_3), 12 ng m^{-3} (NH_4^+), 36 ng m^{-3} (SO_4^{2-}), and 64 ng m^{-3} (NO_3^-). For the convenience of flux calculations, NH_3 values are reported in ng m^{-3} (at STP 100 ng m^{-3} $NH_3 \approx 130$ pptv).

Standard meteorological parameters were measured using a Vaisala HMP45C212 sensor for temperature, an RM Young model 61205V transducer for pressure, and an RM Young Model 05103 wind monitor for wind speed and direction located at the bow ship of the ship at a height

of 8.2 - 9.4 m above the deck. Data were averaged to 1-hour to match the time resolution of the AIM-IC. In order to remove any influence from activities aboard the ship, gas-phase measurements are only reported if the following conditions were met: 1) average hourly ship speed > 4 knots (~7.4 km h^{-1}), 2) average hourly apparent wind direction ± 90° of the bow, and 3) standard deviation of apparent wind direction < 36°. Similar cut-offs for speed and wind direction have been used in previous studies of NH_3 in the marine boundary layer (e.g. Johnson et al., 2008; Norman and Leck, 2005).

2.3 Surface Measurements

A total of 37 surface ocean and 9 melt pond samples were collected throughout the study. Melt pond samples were collected directly into a cooler jug using an electrical pump fixed on a telescopic arm. The water was sampled as far from the side of the melt pond as possible, between 1-2 m depending on the size of the melt pond. Temperature was measured in situ with a VWR high precision thermometer and total aqueous [NH_x] was determined within 10 h of sampling using a fluorometric technique that has been optimized for low concentrations and complex matrices (Holmes et al., 1999). The method detection limit was 20 nM. Surface ocean samples were obtained with a Rosette sampler equipped with GO-FLOW bottles and a CTD (Seabird Electronics SBE911+) recording temperature. Total aqueous [NH_x] was determined as above within 1 hour of sampling. Surface water temperature along the ship's track was continuously measured by a thermosalinograph (Seabird Electronics SBE 45) connected to the seawater inlet. For the purposes of flux calculations, the ocean pH and salinity were assumed to be 8.1 and 35 g kg^{-1}, respectively, which are representative for the region of interest (Takahashi et al., 2014). These assumptions have been made previously and were not found to be a major source of uncertainty when calculating sea-air NH_3 fluxes (Johnson et al., 2008). The melt pond pHs were measured using a pH-meter within four hours of sampling. A three point calibration of the pH probe (Orion™ Model 91-72, Thermo Scientific) was performed using commercially available pH 4.01, 7.00 and 10.00 buffers. Salinity of the melt ponds were determined with a WTW Cond 330i handheld conductivity meter.

2.4 Flux Calculations

The direction of sea-air NH_3 fluxes can be assessed by comparing ambient measurements of $NH_{3(g)}$ to the atmospheric mixing ratio predicted from Henry's Law equilibrium calculations using seawater [NH_x] and surface temperature measurements (e.g. Asman et al., 1994; Johnson

et al., 2008; Quinn et al., 1988, 1996). This equilibrium NH_3 concentration signifies the ambient value at which the net flux changes direction, and is known as the compensation point (denoted χ). In other words, one expects a net downwards flux if ambient $NH_{3(g)}$ exceeds χ and a net upward flux if it is below χ. The magnitude of these fluxes are commonly computed using the "two-phase" model first developed by Liss and Slater (1974), which describes the sea-air transfer of gases as being controlled by molecular diffusion on either side of the interface. The transfer of NH_3 across this interface is predominantly dictated by the air-side transfer velocity, given the relatively high water solubility of NH_3 (Liss, 1983). Hence, the equation to calculate sea-air NH_3 fluxes is:

$$F_{NH3} = k_g \cdot (\chi - NH_{3(g)}) \cdot 17.03 \quad (1)$$

where F_{NH3} is the sea-air flux of NH_3 (ng m^{-2} s^{-1}), k_g is the air-side transfer velocity (m s^{-1}), $NH_{3(g)}$ is the measured ammonia concentration (nmol m^{-3}), χ is the compensation point (nmol m^{-3}), and the molecular weight of 17.03 g mol^{-1} is to convert nmol to ng. Numerous parameterizations exist for k_g with varying degrees of complexity (Johnson, 2010). Here we adopt the approach established by Duce et al. (1991):

$$k_g = \frac{u}{770 + 45 \cdot MW^{1/3}} \quad (2)$$

where u is the wind speed (m s^{-1}) and MW is the molecular weight of the gas of interest (17.03 for NH_3). Although simple, this parameterization has been used previously to estimate sea-air NH_3 fluxes (e.g. Johnson et al., 2008) and has been shown to be in good agreement (within 20 %) with a more complex scheme, particularly at lower wind speeds (Johnson, 2010). The following equation is used to calculate χ:

$$\chi = K_H \cdot [NH_{3(sw)}] \quad (3)$$

where K_H is the Henry's law constant (dimensionless) and $[NH_{3(sw)}]$ is the concentration of dissolved ammonia in the surface pool (nmol m^{-3}). The temperature-dependent equation for K_H is (McKee, 2001):

$$K_H = \frac{1}{17.93 \cdot \frac{T}{273.15} \cdot e^{(4092/T) - 9.70}} \quad (4)$$

where T is the surface temperature (in K). The following equation is used to relate the $NH_{3(sw)}$ to the concentration of total dissolved NH_x ($[NH_{x(sw)}]$), which is the value actually measured by the procedure outlined in section 2.3:

$$[NH_{3(sw)}] = \frac{[NH_{x(sw)}] \cdot K_a}{10^{-pH} + K_a} \quad (5)$$

where K_a is the acid dissociation constant of NH_4^+. The pK_a ($\equiv -\log K_a$) is calculated according to Bell et al. (2008), which provides an empirical correction for salinity (S, dimensionless) at a given temperature (T, in °C):

$$pK_a = 10.0423 + 0.003071 \cdot S - 0.031556 \cdot T \quad (6)$$

Equations (2) and (4) closely follow that of Johnson et al. (2008) but are sufficiently similar to analogous approaches for calculating K_H and k_g used in other sea-air NH_3 exchange studies (e.g. Asman et al., 1994; Gibb et al., 1999; Quinn et al., 1992). Johnson (2004) reported that fluxes calculated with these various schemes usually agree within 2 %. Melt pond-air exchange was also examined using Eqs. (1) to (6).

2.5 GEOS-Chem

The GEOS-Chem chemical transport model (www.geos-chem.org) is used to aid in the interpretation of the atmospheric measurements. We use GEOS-Chem version 9-02 at 2°x2.5° resolution globally, and with 47 vertical layers between the surface and 0.01 hPa. The assimilated meteorology is taken from the NASA Global Modelling and Assimilation Office (GMAO) Goddard Earth Observing System version 5.11.0 (GEOS-FP) assimilated meteorology product. Boundary layer mixing uses the non-local scheme implemented by Lin and McElroy (2010). Our simulations use 2014 meteorology and allow a 2-month spin-up prior to the simulation.

The GEOS-Chem model includes a detailed oxidant-aerosol tropospheric chemistry mechanism as originally described by Bey et al. (2001). Simulated aerosol species include sulphate-nitrate-ammonium (Park et al., 2004; Park et al., 2006), carbonaceous aerosols (Park et al., 2003; Liao et al., 2007), dust (Fairlie et al., 2007; Fairlie et al., 2010) and sea salt (Alexander et al., 2005). The sulphate-nitrate-ammonium chemistry uses the ISORROPIA II thermodynamic model (Fountoukis and Nenes, 2007), which partitions ammonia and nitric acid between the gas and aerosol phases. For our simulations, the natural NH_3 emissions are from Bouwman et al. (1997)

and biomass burning emissions are from the Quick Fire Emissions Dataset (QFED2) (Darmenov and da Silva, 2013), which provides daily open fire emissions at 0.1° x 0.1° resolution. Anthropogenic NH_3 emissions are from Bouwman et al. (1997). The model includes natural and anthropogenic sources of SO_2 (van Donkelaar et al., 2008; Fischer et al., 2011) and DMS emissions based on the Nightingale (2000) formulation and oceanic DMS concentrations from Lana et al. (2011). Oxidation of SO_2 occurs in clouds by reaction with H_2O_2 and O_3 and in the gas phase with OH (Alexander et al., 2009) and DMS oxidation occurs by reaction with OH and NO_3.

GEOS-Chem simulates both wet and dry removal of aerosols and gases. Dry deposition follows a standard resistance in series scheme (Wesley, 1989) with an aerosol dry deposition velocity of 0.03 cm s^{-1} over snow and ice (Fischer et al., 2011). Wet removal in GEOS-Chem takes place in large-scale clouds and convective updrafts (Liu et al., 2001). In-cloud scavenging of hydrophilic species takes place at temperatures warmer than 258K, and hydrophobic black carbon and dust are also removed at temperatures colder than 258K (Wang et al., 2011).

2.6 FLEXPART-WRF

FLEXPART-WRF (Brioude et al., 2013, website: flexpart.eu/wiki/FpLimitedareaWrf) is a Lagrangian particle dispersion model based on FLEXPART (Stohl et al., 2005) that is driven by meteorology from the Weather Research and Forecasting (WRF) Model (Skamarock et al., 2005). Here we use FLEXPART-WRF run in backward mode to study the emissions source regions and transport pathways influencing ship-based ammonia measurements. A WRF simulation for the summer 2014 NETCARE campaign was performed using WRF 3.5.1 with initial and boundary conditions provided by the operational analysis (0.25° x 0.25° resolution) from European Centre for Medium-Range Weather Forecasts (ECMWF). Parameterizations and options for the WRF simulations are given in Table 1. The WRF model was run from 1 July 2014 to 13 August 2014 and nudged to ECMWF winds, temperature, and humidity every 6 hours above the atmospheric boundary layer. The WRF run was evaluated using meteorological measurements made onboard the Amundsen and from Polar-6 aircraft flights during this period. FLEXPART-WRF was run in backward mode to produce retroplume output that is proportional to the residence time of the particles in a given volume of air. Runs were performed using the location of the ship, with one model run performed every 15 minutes while the ship was in the model domain (13 July-13 August 2014). For each run, 100,000 particles were released at the ship location (100 m extent horizontally and vertically) and the

FLEXPART-WRF was run backwards for 7 days prior to release. The output provides retroplume information (the residence time of air prior to sampling) which is used to calculate the potential emission sensitivites (PES) integrated over the seven days prior to sampling by instruments aboard the Amundsen.

3 Results and Discussion

3.1 Surface-Atmosphere NH_3 Fluxes

Figure 1 shows the ambient $NH_{3(g)}$ concentrations measured by the AIM-IC throughout the cruise. Measured values of $NH_{3(g)}$ range between 30-650 ng m^{-3} with the highest values occurring in Lancaster Sound as the ship was steaming eastward into Baffin Bay. Only two measurements of NH_3 were below the detection limit (29 ng m^{-3}) throughout the entire cruise. NH_3 consistently exceeded 100 ng m^{-3} during later parts of the cruise along the eastern shores of Ellesmere Island and western shores of Greenland. Lower values (<100 ng m^{-3}) were observed at the beginning of the campaign along the eastern shores of Baffin Island. Measurements of $NH_{3(g)}$ in the marine boundary layer at northern latitudes (>50°N) are sparse; however the concentrations measured in this study are within the few previously reported ranges for the regions above 50 °N. Johnson et al. (2008) reported $NH_{3(g)}$ between 20-300 ng m^{-3} in the Norwegian Sea during spring and summer, but a lower range (20-90 ng m^{-3}) in the northern North Sea in winter. In the southern North Sea, Asman et al. (1994) measured higher values (30-1500 ng m^{-3}) in a study lasting from February to October.

The relevant measurements needed to calculate χ for both the open ocean and melt ponds are listed in Tables S1 and S2, respectively. Only four unique co-ordinates are listed for the nine melt pond samples because multiple melt ponds were sampled at each location. Roughly half of the surface ocean samples had $[NH_x]$ below the detection limit (20 nM) and in general values were significantly lower than in the melt ponds. Open ocean samples ranged from <20 to 380 nM whereas seven of the nine melt pond samples were between 640 to 1260 nM (with the other two below detection limit). These concentrations and their spatial variability are typical for the region during summer (Martin et al. 2010).

Parameters listed in Tables S1 and S2 were input into Eqs. (3) to (6) to calculate χ for both the surface ocean and melt pond samples. For samples with $[NH_x]$ below the detection limit, a value of 10 nM (half of the detection limit) was assumed. A comparison of the calculated compensation points for the ocean (χ_{ocean}) and melt ponds (χ_{MP}) are shown in Fig. 2. Also shown

is the range for the nearest valid measurement (see section 2.2) of ambient $NH_{3(g)}$. The $NH_{3(g)}$ concentration taken during the hour of surface sampling could not be used since the ship remained stationary for up to 12 hours while melt pond or ocean work was being conducted. Hence, the $NH_{3(g)}$ measurement from several hours prior (as the ship approached the surface sampling site) had to be used. This approach should not significantly impact the analysis given that the ambient levels of $NH_{3(g)}$ were observed to be fairly uniform from one hour to the next (i.e. no rapid spikes of $NH_{3(g)}$ were measured). Shown in lighter yellow are the ranges of $NH_{3(g)}$ observed over the entire study (~30-650 ng m^{-3}). Figure 2 clearly shows that the ambient concentrations of $NH_{3(g)}$ exceed both χ_{ocean} and χ_{MP} by several orders of magnitude throughout the entire region. This conclusively demonstrates that during the summertime, the ocean and melt ponds are net sinks of atmospheric $NH_{3(g)}$. This finding is consistent with Johnson et al. (2008) who found a tendency for downward net fluxes at higher latitudes, primarily as a result of colder sea surface temperatures. Assuming an upper limit for the ocean pH of 8.2 would increase χ_{ocean} by less than 20 %.

Figure 3 shows the magnitude of the sea-air and melt pond-air flux of NH_3. Average net downward fluxes of 1.4 ng m^{-2} s^{-1} and 1.1 ng m^{-2} s^{-1} were calculated for the open ocean and melt ponds, respectively using Eqs. (1) and (2). Net fluxes were exclusively downwards (net deposition into the ocean and melt ponds) due to the relative abundances of $NH_{3(g)}$ and $NH_4^+{}_{(aq)}$ in these surface pools as well as cold surface temperatures as suggested by Johnson et al., (2008). It is unlikely that this represents a significant input of NH_4^+ into the open ocean except in cases of extremely low [NH_x]. A simple calculation assuming a mixed layer depth of 25 m results in an increase of only ~0.3 nM d^{-1} to the ocean (assuming complete mixing and no loss pathways). However, for the much shallower melt ponds (assumed depth of 0.25 m) the same calculation yields an input of ~22 nM d^{-1}. Furthermore, this does not account for atmospheric inputs from either wet deposition or dry deposition of particulate NH_4^+, and these melt ponds are cut-off from the upwelling currents in the ocean which deliver reactive N to the surface. Rates of nitrification, mineralization and N_2-fixation in the open ocean and melt ponds would help put this atmospheric input into perspective and give insight as to whether or not it is an important process in the nitrogen cycle in these environments.

3.2 Sulphate Neutralization

The extent of neutralization of $PM_{2.5}$ influences aerosol properties as discussed previously. Figure 4 depicts the relative abundances (in neq m^{-3}) of gas-phase ammonia and particulate-

phase ammonium and sulphate. It is important to note that the value for sulphate is total $PM_{2.5}$ sulphate as opposed to non-sea salt sulphate (nss-SO_4^{2-}), which is commonly reported for marine boundary layer studies. High and variable backgrounds of Na^+ from the AIM-IC prevented the calculation of nss-SO_4^{2-}, hence this dataset provides an upper limit for nss-SO_4^{2-}. Given the low wind speeds (< 5 m s^{-1}) that dominated the campaign, it is likely the nss-SO_4^{2-} ≈ SO_4^{2-} since the contribution from sea salt to $PM_{2.5}$ was likely small. It should also be noted that measurements of SO_2, HNO_3 and NO_3^- were almost always below their respective detection limits.

Particle loadings of NH_4^+ and SO_4^{2-} were extremely low (typically < 5 neq m^{-3}) throughout the duration of the cruise. During the first third of the cruise (before 18 July), gas-phase NH_3 was also low and neutralization (i.e. the ratio NH_4^+:SO_4^{2-} in units of equivalents) was ambiguous due to numerous values near or below detection limit. On the other hand, after 25 July the nanoequivalents of $NH_{3(g)}$ were substantially higher than either NH_4^+ or SO_4^{2-} (i.e. $NH_x \approx NH_3$), which implies a nearly neutralized sulphate aerosol. It is important to note that a nearly neutralized aerosol does not equate to an aerosol with a pH of 7 since aerosol pH is highly sensitive to liquid water content as well as the precise NH_4^+:SO_4^{2-} ratio. An aerosol with NH_4^+:SO_4^{2-} approaching 1 can still have an acidic pH. For example, a deliquesced ammonium sulphate particle containing 20 neq m^{-3} of SO_4^{2-} and 19.98 neq m^{-3} NH_4^+ at 85% RH will have a pH of ~3.1 under equilibrium conditions despite having an NH_4^+:SO_4^{2-} equivalents ratio of 0.999.

Figure 5 shows the distribution of the NH_4^+:nss-SO_4^{2-} ratio (on a per equivalent basis) measured at Alert, Nunavut (82.50 °N, 62.33 °W) as a function of month from 1996-2011. Weekly-averaged $PM_{2.5}$ speciation measurements at Alert are made by Environment Canada and are available on-line (Environment Canada, 2014). The contribution from NO_3^- is minor and has not been included in this analysis. In warm environments volatilization of NH_4NO_3 off of filters can cause an underestimation of NH_4^+, but this is not expected to be an issue at Alert due to cold weather and low loadings of NH_4NO_3. During July and August the nss-SO_4^{2-} is, on average, completely neutralized by the NH_4^+ in $PM_{2.5}$ as shown by a median neutralization ratio approaching 1 during these months. This implies there is sufficient $NH_{3(g)}$ throughout the region to neutralize nss-SO_4^{2-} produced from DMS oxidation which is consistent with the measurements shown in Fig. 4. However, there is no denuder upstream of the Hi-Vol filters to remove NH_3 so the observed NH_4^+:SO_4^{2-} ratio (Fig. 5) may be higher than for ambient $PM_{2.5}$.

This effect is difficult to characterize, but if it is important then it is still evidence for the abundance of NH_3 in the summertime Arctic boundary layer. Lastly, Johnson and Bell (2008) show that a sufficiently neutralized sulphate aerosol will tend to 'push' gas-phase NH_3 into the ocean in the aerosol-gas-ocean system, also consistent with Fig. 3. The AIM-IC and Alert measurements are both inconsistent with a previous study that used GEOS-Chem to predict a highly acidic aerosol and insignificant gas-phase ammonia ($NH_x \approx NH_4^+$) throughout the summertime Arctic marine boundary layer (Breider et al., 2014). This inconsistency implies a missing process in a widely used CTM that we investigate further below.

3.3 Evidence for the Importance of Seabird Guano

Observations collected on board the Amundsen and at Alert strongly suggest a significant source of NH_3 in the Baffin Bay region. Decomposition of uric acid in seabird guano (excreta) has been recognized as a significant source of NH_3 where large colonies exist (Blackall et al., 2007; Wilson et al., 2004). However, studies measuring NH_3 from seabird colonies are limited due to the remoteness of most colonies and technical challenges in quantifying NH_3 in isolated locations (Blackall et al., 2007). The few studies that have been done have focused on colonies located in the United Kingdom (Blackall et al., 2004; Wilson et al., 2004), Antarctica (e.g. Legrand et al., 1998; Zhu et al., 2011) and remote tropical islands (Riddick et al., 2014; Schmidt et al., 2010). Recently, Riddick et al. (2012) developed a global inventory to estimate the magnitude and spatial distribution of $NH_{3(g)}$ from seabird guano. The authors employed a bioenergetics model, first developed by Wilson et al. (2004), to calculate the $NH_{3(g)}$ emissions (in g $bird^{-1}$ yr^{-1}) for 323 different seabird species. After compiling a list detailing the populations and locations of 33,225 colonies, they were able to estimate global annual emissions between 97-442 Gg NH_3 per year. Although this is less than 2% of total global $NH_{3(g)}$ emissions, it can be the dominant source in remote regions where seabird populations are large and other sources are negligible.

In order to assess the impact of seabird guano on NH_3 across the Baffin Bay region, seabird colony NH_3 emissions were implemented in the GEOS-Chem model, and the impact on monthly mean surface layer NH_3 was examined. The NH_3 emissions inventory used in the standard GEOS-Chem v9-02 (and in many other CTMs) is from Bouwman et al. (1997) and does not include seabird emissions. Paulot et al. (2015) recently showed the oceanic emissions from this original inventory are roughly a factor of 3 too high since the initial inventory assumes atmospheric NH_3 is equal to zero. The Riddick et al. (2012, 2012b) seabird colony NH_3

emissions inventory (scenario 3) was added to the original inventory in GEOS-Chem following Paulot et al. (2015). Scenario 3 was chosen since this represented the midpoint between the minimum and maximum emissions of scenario 1 and 2, respectively. Close inspection of this seabird inventory revealed that some large seabird colonies in our study region were not accounted for. To investigate this, the spatial co-ordinates of northern colonies (>50 °N) in the Riddick et al. (2012) inventory were cross-referenced against colonies in the on-line Circumpolar Seabird Data Portal (Seabird Information Network, 2015). Annual emissions for large colonies in the seabird data portal were calculated in the same manner as in Riddick et al. (2012). In total, there were 42 colonies present in the seabird data portal but absent in the Riddick inventory in the region north of 50 °N. These additional emissions were added to the inventory we implemented in GEOS-Chem. These colonies totaled 7.5 Gg NH_3 $year^{-1}$ (approximately one quarter of the existing emissions north of 50 °N) and were primarily in Siberia and western Alaska. The Riddick et al. (2012) bioenergetics model only counts emissions that occur during breeding season and while the seabirds are at the colony. Hence, the annual emission estimates (Gg NH_3 $year^{-1}$) per colony were temporally allocated evenly between the 15 May to 15 September. This period is when the majority of seabirds in the Baffin Bay region are nesting (e.g. Gaston et al., 2005; Mallory and Forbes, 2007; McLaren, 1982). One limitation to this approach is that it does not account for additional temporal variations in NH_3 emissions. For instance, moisture increases the rate of uric acid degradation, and fluxes of NH_3 from guano have been observed to increase 10-fold for up to a day after rain events (Riddick et al., 2014).

Figure 6 shows the July mean output for surface layer NH_3 mixing ratio both without (Fig. 6a) and with (Fig. 6b) seabird emissions, along with the $NH_{3(g)}$ measured by the AIM-IC denoted by circles in Fig. 6a. Comparing the top two panels reveals that seabird emissions make a substantial impact on modelled NH_3 levels in the boundary layer. Much better model-measurement agreement is achieved with the inclusion of the seabird colonies. Without the seabird emissions, NH_3 mixing ratios are underpredicted by several orders of magnitude. Surface NH_3 is still underpredicted in Fig. 6b (with guano NH_3 emissions) which could be the result of modelled emissions being independent of rainfall, which can substantially increase NH_3 emissions. Episodic rainfall was persistent throughout the latter half of the campaign. Other contributing factors may include: challenges in representing boundary layer mixing, uncertainties in deposition rates, comparing monthly averages (GEOS-Chem) to ambient hourly measurements, missing/underestimated bird colonies, and/or excreta from other fauna (e.g.

seals, caribou, musk-ox) absent in the updated inventory. The bottom two panels (Figs. 6c and 6d) show the influence of seabirds on the ammonium to non-sea salt sulphate ratio. Without seabirds (Fig. 6c) the ratio is less than 0.3 throughout most of the study region, which is inconsistent with the abundance of NH_3 relative to SO_4^{2-} measured by the AIM-IC. Adding the seabird emissions (Fig. 6d) increases the ratio to above 0.7 in most grid cells along the ship track. Although the high ratio (July average is ~1) observed at Alert (denoted by the star in Figs. 6c and 6d) is underestimated in the GEOS-Chem simulation, the bias is reduced by nearly a factor of 2 (from 0.32 to 0.57) when seabird emissions are included.

Wildfires are also a source of NH_3 to the free troposphere and/or boundary layer. Particularly strong wildfire events were persistent in the Northwest Territories (NWT) during the study period. Blue circles in Fig. 7 show the location and average fire radiative power (representative of fire strength) of wildfires across the Arctic from July 20-26. It was constructed using data from NASA's Fire Information Resource Management System (FIRMS) database (NASA, 2015). We used FLEXPART-WRF retro plumes to assess the importance of wildfire NH_3 emissions, as well as to further corroborate the influence of seabird guano.

The significant impact of seabird colonies on $[NH_{3(g)}]$ is supported by the analysis of FLEXPART-WRF retro plumes shown in Fig. 7. Periods of low $[NH_{3(g)}]$ (bottom panel in Fig. 7) correspond to air masses that spent at least the last 48 hours over the ocean and/or aloft above the MBL (~500 m) where NH_3 sources are negligible. This is clearly shown in Fig. 7a where the air mass sampled on 14 July 00:00 (UTC) spent the previous 96 hours in the MBL over Baffin Bay, consistent with low $[NH_{3(g)}]$. In contrast, on 26 July 00:00 (Fig. 7b) air had recently passed over seabird colonies (purple circles) surrounding Lancaster Sound as well as wildfires in the Northwest Territories (NWT) on mainland Canada (blue circles), coincident with the large increase in $[NH_{3(g)}]$. A similar $NH_{3(g)}$ peak occurs on 3 August that can also be examined by using a retro plume analysis. Low $NH_{3(g)}$ values observed on the morning of 2 August agree with Fig. 7c showing the air originating from the MBL over Baffin Bay. At 3 August 00:00 (Fig. 7d) the air had spent the last 12 hours in the boundary layer of Western Greenland where large seabird colonies exist. However, by 4 August 00:00 (Fig. 7e) the retro plume shifted such that air is now originating from primarily above the boundary layer (altitude plots not shown) leading to a decrease in $NH_{3(g)}$. In addition from August 2-4 the ship was north of 79° N and in the Eastern Canadian Arctic, hence it is unlikely that this increase in NH_3 can be attributed to wildfires given how far removed this region is from wildfires in the NWT. While Fig. 7 only

highlights five examples from the study period, retro plumes throughout the entire campaign also support the hypothesis that $NH_{3(g)}$ in the MBL originates primarily from seabird colonies (for the Eastern Canadian Arctic) with contributions from wildfires in some regions (central Canadian Arctic). All $NH_{3(g)}$ spikes in the time series can be attributed to air that had recently passed over seabird colonies and/or wildfires, whereas low values coincide with air masses from either the open ocean or free troposphere not influenced by wildfires.

To further investigate the potential influence of wildfires on NH_3 in the Arctic MBL, GEOS-Chem simulations were performed using a wildfire emissions inventory for 2014 (QFED2). Simulations with/without wildfires and with/without seabirds revealed that in Lancaster Sound (along 74° N) roughly 40% and 55% of the boundary layer NH_3 can be attributed to seabirds and wildfires, respectively. In other words, air sampled in Lancaster Sound (20 July to 27 July) was likely influenced by wildfires in NWT in addition to seabird guano. On the other hand, north of Lancaster Sound, contributions from seabirds and wildfires to surface layer NH_3 were approximately 95% and 5%, respectively. Wildfires in the NWT are an important but episodic source of summertime NH_3 in the Canadian Arctic. This is due to periodic transport events associated with this source that is located remote to our study region. Whereas, seabird colonies are a local, and persistent source of NH_3 from May to September. Given the observation of consistently neutralized sulfate at Alert each summer, and the large interannual variability and episodic wildfire influence, emissions from migratory seabirds are likely to be a significant contributor to NH_3 abundance in the Arctic marine boundary layer.

3.4 Implications for N-deposition to Ecosystems

Previous studies have highlighted the important role that seabird-derived N can play in the nitrogen cycle of ecosystems adjacent to bird colonies due to large deposition rates of NH_3 and NH_4^+ (e.g. Anderson and Polis, 1999; Lindeboom, 1984). However, little attention has been paid to the effects of seabird-derived N on deposition at the regional scale. In this section, we consider the importance of seabird-derived nitrogen as an input of reactive N to Arctic ecosystems. These ecosystems tend to be N-limited during the summer and hence have a large sensitivity to N input (Shaver and Chapin III, 1980). In terrestrial ecosystems, soil N availability is a key factor in determining both plant community structure (McKane et al., 2002) and greenhouse gas emissions from soil (Stewart et al., 2012).

Nitrogen (N_2) fixation via microbes is thought to be the primary N input to remote Arctic terrestrial ecosystems (e.g. Cleveland et al., 1999; Hobara et al., 2006; Stewart et al., 2014). Numerous field studies have been conducted to estimate N_2-fixation rates via the acetylene reduction technique (Hardy et al., 1968). The N_2-fixation rates for most terrestrial Arctic sites fall within the range of 10 to 120 mg N m^{-2} yr^{-1} (Hobara et al., 2006). However, highly variable rates (due to spatial heterogeneity of microbial populations) and assumptions in the acetylene reduction technique yield high degrees of uncertainty for N_2-fixation rates (Stewart et al., 2014).

Total atmospheric N-deposition (wet and dry) in the Arctic is thought to be smaller than fixation, with typical ranges from 8 to 56 mg N m^{-2} yr^{-1} (Van Cleve and Alexander, 1981). Only a few N_2-fixation studies also quantify wet deposition, with dry deposition being ignored altogether (e.g. Hobara et al., 2006). Nonetheless, in certain Arctic regions atmospheric deposition may exceed N_2-fixation in soils (DeLuca et al., 2008). These processes are coupled since large inputs of NH_4^+ have been shown to inhibit N_2-fixation in certain microbial species and lichens (Chapin and Bledsoe, 1992).

Figure 8 shows results from the GEOS-Chem simulation of total NH_x ($\equiv NH_3 + NH_4^+$) deposition (both wet and dry) for the months May to September (inclusive) both without (Fig. 8a) and with (Fig. 8b) seabird NH_3 emissions. The difference in total NH_x deposition for birds and no birds is shown in Fig. 8c (absolute difference) and Fig. 8d (percent difference). Areas near large colonies are heavily influenced by seabird guano with NH_x deposition from seabirds exceeding 10 mg N m^{-2} yr^{-1}, particularly in western Greenland and near the mouth of Lancaster Sound. The majority of NH_x deposition is caused by NH_3 as opposed to NH_4^+. Most regions in Fig. 8b are on the lower end of the annual N-deposition rate of 8 to 56 mg N m^{-2} yr^{-1} suggested by Van Cleve and Alexander (1981). However, there are two important distinctions: the latter is an estimate of total N-deposition and annual input. Estimates in Fig. 8 might be more useful for comparing N-deposition to N_2-fixation since it captures deposition only during the growing season, and NH_x is likely the dominant form of atmospheric reactive N in the summertime Arctic boundary layer. Furthermore, Fig. 8b provides information on regions where N-deposition rates could be comparable to input from terrestrial N_2-fixation (>10 mg N m^{-2} yr^{-1}) which can help inform subsequent studies exploring N-cycling in the region. According to Hobara et al. (2006), Arctic terrestrial N_2-fixation only occurs from May-September (inclusive) and peaks in July, similar to migration patterns of Arctic seabirds.

Estimates of N_2-fixation rates in the Arctic Ocean mixed layer are even sparser than estimates for terrestrial ecosystems. To our knowledge, only Blais et al. (2012) have measured oceanic N_2-fixation in the summertime Arctic Ocean mixed layer. The authors found that open ocean N_2-fixation rates averaged 0.12 nM d^{-1} in the upper 50 m of the water column throughout the Beaufort Sea to Baffin Bay. For the period of May to September (inclusive) this represents an input of approximately 13 mg N m^{-2} which is comparable to inputs we calculate from guano-derived NH_3 in regions close to seabird colonies as shown in Fig. 8b.

4 Conclusions

Simultaneous measurements of atmospheric and oceanic composition in the eastern Canadian Arctic revealed that the summertime Arctic Ocean and melt ponds were net sinks of $NH_{3(g)}$. Concentrations of $NH_{3(g)}$ ranging from 30-650 ng m^{-3} were observed and represent the first reported measurements of $NH_{3(g)}$ in the Canadian Arctic. An average downward flux of 1.4 ng m^{-2} s^{-1} into the Arctic Ocean was calculated, consistent with previous studies showing that higher latitude waters are a net NH_3 sink (Johnson et al., 2008). Melt ponds had a smaller net downward flux (1.1 ng m^{-2} s^{-1}) as well as a slightly higher χ as compared to the open ocean (median 2 ng m^{-3} versus 0.8 ng m^{-3}). To our knowledge, this is the first study to estimate melt pond-air NH_3 exchange despite the ubiquitous presence of melt ponds throughout the summertime Arctic.

On a nanoequivalent basis, $NH_{3(g)}$ values were significantly greater (up to an order of magnitude more) than both NH_4^+ and SO_4^{2-}. This finding was consistent with a 15-year historical dataset of weekly $PM_{2.5}$ composition from Alert, NU which showed that nss-SO_4^{2-} is, on average, completely neutralized by NH_4^+ during July and August. These measurements imply strong regional source(s) of $NH_{3(g)}$ in the eastern Canadian Arctic Archipelago that are sufficient to neutralize nss-SO_4^{2-} produced from DMS oxidation. Our surface-air flux estimates show that the Arctic Ocean and melt ponds are not responsible for $NH_{3(g)}$ in the marine boundary layer.

It is also noteworthy that even though these melt ponds have significantly higher [NH_x] than the open ocean (average of 670 nM versus 55 nM), χ_{MP} is only marginally higher. More acidic pHs and slightly lower temperatures mitigate the effect of higher [NH_x] on χ. Chemical transport models (CTMs) that explicitly account for bi-directional NH_3 exchange typically require χ as a predefined model input (e.g. Bash et al., 2013; Wichink Kruit et al., 2012). Therefore, from a modelling standpoint, similar values of χ_{ocean} and χ_{MP} are convenient since they can be parameterized in a similar fashion which would remove the need for CTMs to

resolve the spatial extent and temporal evolution of melt ponds to properly model surface-atmosphere NH_3 exchange in the summertime Arctic.

To investigate the impact of NH_3 emissions from seabird guano, we examined GEOS-Chem simulations both with and without seabird colony NH_3 emissions. The seabird NH_3 emission inventory developed by Riddick et al. (2012) was updated for this study to include northern colonies (>50 °N) that had been overlooked in the original inventory. Without the seabirds, GEOS-Chem underestimated $NH_{3(g)}$ by several orders of magnitude and predicted highly acidic aerosol at the surface in July, which is in direct contrast to our measurements. The inclusion of seabird emissions provided much better agreement with $NH_{3(g)}$ observations and yielded more neutralized aerosol throughout most of the Baffin Bay region. The importance of seabird NH_3 emissions is also supported by analysis of FLEXPART-WRF retro plumes throughout the study period. Air masses enriched in $NH_{3(g)}$ had recently passed through regions with seabird colonies whereas periods of low $NH_{3(g)}$ involved air masses originating from the open ocean or above the boundary layer. Together, these models provide strong evidence that seabird colonies are the dominant and persistent local source of $NH_{3(g)}$ in the summertime Arctic. FLEXPART-WRF and GEOS-Chem were also used to assess the influence of wildfires on NH_3. Wildfires are an important but episodic source of NH_3 source to the Arctic due to ongoing changes in transport patterns and fire intensity. Further work should be done to examine the inter-annual influence of NH_3 emissions from wildfires in the NWT on other regions in the Arctic.

Deposition estimates of NH_x from GEOS-Chem during the seabird nesting season (May to September) exceed 10 mg N m^{-2} $season^{-1}$ in grid cells close to large seabird colonies, which is on the lower end of microbial N_2-fixation in Arctic tundra (Hobara et al., 2006). Hence, in some regions seabird-derived NH_x could be a significant N-input to terrestrial Arctic ecosystems which are typically very N-sensitive. Estimates of NH_3 fluxes into the open ocean are unlikely to be an important input of reactive-N except for waters close to large seabird colonies; however, these fluxes may be important for the N-cycle in the much shallower melt ponds.

There is strong evidence that seabird colonies are likely the dominant and persistent source of $NH_{3(g)}$ to the summertime Arctic boundary layer. Emissions appear to be significant enough to at least partially neutralize nss-SO_4^{2-} throughout most of the study region, in contrast to previous model simulations that did not consider seabird colony emissions. Further research is required to better constrain the location, population, and NH_3 emissions of Arctic seabird colonies. It is also important to quantify meteorological effects (e.g. rainfall, wind speed) on seabird

emissions. The NH_3 emissions inventory in CTMs should be updated to include seabird emissions with correct representation of the breeding season so that emissions only occur when seabirds are nesting. Summertime measurements of atmospheric NH_x elsewhere in the Arctic are needed to assess whether the impacts of seabirds observed in this study (substantial $NH_{3(g)}$, nss-SO_4^{2-} neutralization, and N-deposition) are relevant to the entire Arctic.

Acknowledgements

The authors are grateful for the hard work and dedication of the CCGS *Amundsen* crew. The authors also thank E. Mungall, A. Lee, V. Irish, H. Stark and J. J. B. Wentzell for help during mobilization, demobilization and calibration of the AIM-IC, as well as T. Papakyriakou and T. Burgers for providing meteorological data. The GEOS5-FP data used in this study/project have been provided by the Global Modeling and Assimilation Office (GMAO) at NASA Goddard Space Flight Center. The hi-volume sampler used for the Alert measurements was maintained and calibrated by D. Veber, as well as numerous other technicians and operators over the years. Acknowledgement is also extended to the crew at CFS Alert for maintaining the base year round. The fieldwork and model analysis was supported by NSERC's Climate Change and Atmospheric Research program, ArcticNet and NSERC. The QFED2 code and emissions data was provided by K. Travis and P. Kim. The NASA FIRMS data set was provided by LANCE FIRMS operated by NASA/GSFC/ESDIS with funding provided by NASA/HQ. G. R. W. acknowledges funding from the NSERC program Integrating Atmospheric Chemistry from Earth to Space (IACPES). Lastly, the authors wish to thank B. Christensen for providing logistical support throughout the project.

References

Abbatt, J. P. D., Benz, S., Cziczo, D. J., Kanji, Z., Lohmann, U. and Möhler, O.: Solid Ammonium Sulfate Aerosols as Ice Nuclei: A Pathway for Cirrus Cloud Formation, Science, 313, 1770–1773, 2006.

Anderson, W. B. and Polis, G. A.: Nutrient fuxes from water to land : seabirds affect plant nutrient status on Gulf of California islands, Oecologia, 118, 324–332, doi:10.1007/s004420050733, 1999.

Asman, W. A. H., Harrison, R. M. and Ottley, C. J.: Estimation of the net air-sea flux of ammonia over the southern bight of the North Sea, Atmos. Environ., 28(22), 3647–3654, doi:10.1016/1352-2310(94)00192-N, 1994.

Bash, J. O., Cooter, E. J., Dennis, R. L., Walker, J. T. and Pleim, J. E.: Evaluation of a regional air-quality model with bidirectional NH_3 exchange coupled to an agroecosystem model, Biogeosciences, 10(3), 1635–1645, doi:10.5194/bg-10-1635-2013, 2013.

Bell, T. G., Johnson, M. T., Jickells, T. D. and Liss, P. S.: Ammonia/ammonium dissociation coefficient in seawater: A significant numerical correction, Environ. Chem., 5(3), 183–186, doi:10.1071/EN07032, 2008.

Blackall, T. D., Theobald, M. R., Milford, C., Hargreaves, K. J., Nemitz, E., Wilson, L. J., Bull, J., Bacon, P. J., Hamer, K. C., Wanless, S. and Sutton, M. A.: Application of tracer ratio and inverse dispersion methods with boat-based plume measurements to estimate ammonia emissions from seabird colonies, Water, Air, Soil Pollut. Focus, 4(6), 279–285, doi:10.1007/s11267-004-3038-9, 2004.

Blackall, T. D., Wilson, L. J., Theobald, M. R., Milford, C., Nemitz, E., Bull, J., Bacon, P. J., Hamer, K. C., Wanless, S. and Sutton, M. A.: Ammonia emissions from seabird colonies, Geophys. Res. Lett., 34(10), 1–5, doi:10.1029/2006GL028928, 2007.

Blais, M., Tremblay, J.-É., Jungblut, A. D., Gagnon, J., Martin, M. and Lovejoy, C.: Nitrogen flixation and identification of potential diazotrophs in the Canadian Arctic, Global Biogeochem. Cycles, 26, GB3022, 2012.

Bouwman, A. F., Lee, D. S., Asman, W. A. H., Dentener, F. J., Van Der Hoek, K. W., Olivier, J. G. J. and Tg, N.: A global high-resolution emission inventory for ammonia, Global Biogeochem. Cycles, 11(4), 561–587, 1997.

Breider, T. J., Mickley, L. J., Jacob, D. J., Wang, Q., Fisher, J. A., Chang, R. Y.-W. and Alexander, B.: Annual distributions and sources of Arctic aerosol components, aerosol optical depth, and aerosol absorption, J. Geophys. Res. Atmos., 119, 4107–4124, doi:10.1002/2013JD020996, 2014.

Brioude, J., Arnold, D., Stohl, A., Cassiani, M., Morton, D., Seibert, P., Agevine, W., Evan, S., Dingwell, A., Fast, J. D., Easter, R. C., Pisso, I., Burkhart, J., and Wotawa, G.: The Lagrangian particle dispersion model FLEXPART-WRF version 3.1., Geosci. Model Dev., 6, 1889-1904, doi:10.5194/gmd-6-1889-2013, 2013.

Carpenter, L. J., Archer, S. D. and Beale, R.: Ocean-atmosphere trace gas exchange, Chem. Soc. Rev., 41, 6473–6506, doi:10.1039/c2cs35121h, 2012.

Chang, R. Y.-W., Leck, C., Graus, M., Müller, M., Paatero, J., Burkhart, J. F., Stohl, A., Orr, L. H., Hayden, K., Li, S. M., Hansel, A., Tjernström, M., Leaitch, W. R. and Abbatt, J. P. D.: Aerosol composition and sources in the central Arctic Ocean during ASCOS, Atmos. Chem. Phys., 11(20), 10619–10636, doi:10.5194/acp-11-10619-2011, 2011.

Chapin, D. M. and Bledsoe, C.: Nitrogen fixation in arctic plant communities, in Arctic Ecosystems in a Changing Climate: An Ecophysiological Perspective, edited by R. S. Chapin III, R. L. Jeffries, J. F. Reynolds, G. R. Shaver, and J. Svoboda, pp. 301–319, Academic Press, San Diego., 1992.

Chou, M.-D. and Suarez, M. J..: An efficient thermal infrared radiation parameterization for use in general circulation models, National Aeronautics and Space Administration, NASA Tech. Memo, 84 pp., 1994.

Cleveland, C. C., Townsend, A. R., Schimel, D. S., Fisher, H., Hedin, L. O., Perakis, S., Latty, E. F., Fischer, C. Von, Elseroad, A. and Wasson, M. F.: Global patterns of terrestrial biological nitrogen (N_2) fixation in natural ecosystems, Global Biogeochem. Cycles, 13(2), 623–645, doi:10.1029/1999GB900014, 1999.

Darmenov, A. and da Silva, A.: The Quick Fire Emissions Dataset (QFED) – Documentation of versions 2.1, 2.2 and 2.4, NASA Technical Report Series on Global Modeling and Data Assimilation, NASA TM-2013-104606, 32, 183 pp., Draft Document (12939 kB), 2013.

DeLuca, T. H., Zackrisson, O., Gundale, M. J. and Nilsson, M.-C.: Ecosystem feedbacks and nitrogen fixation in boreal forests., Science, 320, 1181, doi:10.1126/science.1154836, 2008.

Duce, R. A., Liss, P. S., Merrill, J. T., Atlas, E. L., Buat-Menard, P., Hicks, B. B., Miller, J. M., Prospero, J. M., Arimoto, R., Church, T. M., Ellis, W., Galloway, J. N., Hansen, L., Jickells, T. D., Knap, A. H., Reinhardt, K. H., Schneider, B., Soudine, A., Tokos, J. J., Tsunogai, S., Wollast, R. and Zhou, M.: The atmospheric input of trace species to the world ocean, Global Biogeochem. Cycles, 5(3), 193–259, doi:10.1029/91GB01778, 1991.

Environment Canada: Canadian Aerosol Baseline Measurement (CABM) Data, [online] Available from: http://www.ec.gc.ca/donneesnatchem-natchemdata/default.asp?lang=En&n=22F5B2D4-1 (Accessed 7 May 2015), 2014.

Fickert, S., Adams, J. W. and Crowley, J. N.: Activation of Br_2 and BrCl via uptake of HOBr onto aqueous salt solutions, J. Geophys. Res., 104, 23719–23727, 1999.

Gaston, A. J., Gilchrist, H. G. and Hipfner, J. M.: Climate change, ice conditions and reproduction in an Arctic nesting marine bird: Brunnich's guillemot (Uria lomvia L.), J. Anim. Ecol., 74(5), 832–841, doi:10.1111/j.1365-2656.2005.00982.x, 2005.

Geernaert, L. L. S., Geernaert, G. L., Granby, K. and Asman, W. A. H.: Fluxes of soluble gases in the marine atmosphere surface layer, Tellus, 50B, 111–127, 1998.

Gibb, S. W., Mantoura, R. F. C. and Liss, P. S.: Ocean-atmosphere exchange and atmospheric speciation of ammonia and methylamines in the region of the NW Arabian Sea, Global Biogeochem. Cycles, 13(1), 161–178, doi:10.1029/98GB00743, 1999.

Hardy, R. W. F., Holsten, R. D., Jackson, E. K. and Burns, R. C.: The Acetylene-Ethylene Assay for N_2 Fixation: Laboratory and Field Evaluation, Plant Physiol., 43, 1185–1207, 1968.

Hobara, S., McCalley, C., Koba, K., Giblin, A. E., Weiss, M. S., Gettel, G. M. and Shaver, G. R.: Nitrogen Fixation in Surface Soils and Vegetation in an Arctic Tundra Watershed: A Key Source of Atmospheric Nitrogen, Arctic, Antarct. Alp. Res., 38(3), 363–372, 2006.

Holmes, R. M., Aminot, A., Kérouel, R., Hooker, B. A and Peterson, B. J.: A simple and precise method for measuring ammonium in marine and freshwater ecosystems, Can. J. Fish. Aquat. Sci., 56(10), 1801–1808, doi:10.1139/f99-128, 1999.

Hong, S.-Y., Dudhia, J. and Chen, S.-H.: A revised approach to ice microphysical processes for the bulk parameterization of clouds and precipitation, Mon. Weather Rev., 132, 103-120, 2004.

Iacono, M. J., Delamere, J. S., Mlawer, E. J., Shephard, M. W., Clough, S. A. and Collins, W. D.: Radiative forcing by long-lived greenhouse gases: Calculations with the AER radiative transfer models, J. Geophys. Res., 113, D13103, 2008.

Janjic, Z. I.: The Step-Mountain Eta Coordinate Model: Further developments of the convection, viscous sublayer, and turbulence closure schemes, Mon. Weather Rev., 122, 927-945, 1994.

Janjic, Z. I.: The surface layer in the NCEP eta Model, in: Eleventh conference on numerical weather prediction, Norfolk, VA, 19-23 August 1996, 354-355, 1996.

Janjic, Z. I.: Nonsingular implementation of the Mellor-Yamada Level 2.5 Scheme in the NCEP Meso model, National Centers for Environmental Prediction, Office Note No. 437, 61 pp., 2002.

Johnson, M. T.: The air-sea flux of ammonia, Ph.D. thesis, University of East Anglia., 2004.

Johnson, M. T.: A numerical scheme to calculate temperature and salinity dependent air-water transfer velocities for any gas, Ocean Sci., 6(4), 913–932, doi:10.5194/os-6-913-2010, 2010.

Johnson, M. T. and Bell, T. G.: Coupling between dimethylsulphide emissions and the ocean-atmosphere exchange of ammonia, Environ. Chem., 5, 259-267, doi:10.107/EN08030, 2008.

Johnson, M. T., Liss, P. S., Bell, T. G., Lesworth, T. J., Baker, A. R., Hind, A. J., Jickells, T. D., Biswas, K. F., Woodward, E. M. S. and Gibb, S. W.: Field observations of the ocean-atmosphere exchange of ammonia: Fundamental importance of temperature as revealed by a comparison of high and low latitudes, Global Biogeochem. Cycles, 22(1), 1–15, doi:10.1029/2007GB003039, 2008.

Kain, J. S.: The Kain-Fritsch convective parameterization: An update, J. Appl. Meteorol., 43, 170-181, 2004.

Kirkby, J., Curtius, J., Almeida, J., Dunne, E., Duplissy, J., Ehrhart, S., Franchin, A., Gagné, S., Ickes, L., Kürten, A., Kupc, A., Metzger, A., Riccobono, F., Rondo, L., Schobesberger, S., Tsagkogeorgas, G., Wimmer, D., Amorim, A., Bianchi, F., Breitenlechner, M., David, A., Dommen, J., Downard, A., Ehn, M., Flagan, R. C., Haider, S., Hansel, A., Hauser, D., Jud, W., Junninen, H., Kreissl, F., Kvashin, A., Laaksonen, A., Lehtipalo, K., Lima, J., Lovejoy, E. R., Makhmutov, V., Mathot, S., Mikkilä, J., Minginette, P., Mogo, S., Nieminen, T., Onnela, A., Pereira, P., Petäjä, T., Schnitzhofer, R., Seinfeld, J. H., Sipilä, M., Stozhkov, Y., Stratmann, F., Tomé, A., Vanhanen, J., Viisanen, Y., Vrtala, A., Wagner, P. E., Walther, H., Weingartner, E., Wex, H., Winkler, P. M., Carslaw, K. S., Worsnop, D. R., Baltensperger, U. and Kulmala, M.: Role of sulphuric acid, ammonia and galactic cosmic rays in atmospheric aerosol nucleation., Nature, 476, 429–433, doi:10.1038/nature10343, 2011.

Krupa, S. V.: Effects of atmospheric ammonia (NH_3) on terrestrial vegetation: A review, Environ. Pollut., 124(2), 179–221, doi:10.1016/S0269-7491(02)00434-7, 2003.

Leaitch, W. R., Sharma, S., Huang, L., Toom-Sauntry, D., Chivulescu, A., Macdonald, A. M., von Salzen, K., Pierce, J. R., Bertram, A. K., Schroder, J. C., Shantz, N. C., Chang, R. Y.-W. and Norman, A.-L.: Dimethyl sulfide control of the clean summertime Arctic aerosol and cloud., Elem. Sci. Anth., 1, doi:10.12952/journal.elementa.000017, 2013.

Leck, C., Nilsson, E. D., Bigg, E. K. and Bäcklin, L.: Atmospheric program on the Arctic Ocean Expedition 1996 (AOE-96): An overview of scientific goals, experimental approach, and instruments, J. Geophys. Res., 106(D23), 32051–32067, doi:10.1029/2000JD900461, 2001.

Lefer, B. L., Talbot, R. W. and Munger, J. W.: Nitric acid and ammonia at a rural northeastern U.S. site, J. Geophys. Res., 104(D1), 1645, doi:10.1029/1998JD100016, 1999.

Legrand, M., Ducroz, F., Wagenbach, D., Mulvaney, R. and Hall, J.: Ammonium in coastal Antarctic aerosol and snow: Role of polar ocean and penguin emissions, J. Geophys. Res., 103, 11043–11056, 1998.

Lin, J.-T. and McElroy, M.: Impacts of boundary layer mixing on pollutant vertical profiles in the lower troposphere: Implications to satellite remote sensing, Atmos. Environ. 44(14), 1726-1739, doi:10.1016/j.atmosenv.2010.02.09, 2010.

Lindeboom, H. J.: The Nitrogen Pathway in a Penguin Rookery, Ecology, 65(1), 269–277, 1984.

Liss, P. S.: Gas transfer: Experiments and geochemical implications, in Air-Sea Exchange of Gases and Particles, edited by P. S. Liss and W. G. N. Slinn, pp. 241–298, Springer Netherlands., 1983.

Liss, P. S. and Slater, P. G.: Flux of Gases across the Air-Sea Interface, Nature, 247, 181–184, doi:10.1038/247181a0, 1974.

Lüthje, M., Feltham, D. L., Taylor, P. D. and Worster, M. G.: Modeling the summertime evolution of sea-ice melt ponds, J. Geophys. Res. Ocean., 111, C02001, doi:10.1029/2004JC002818, 2006.

Mallory, M. L. and Forbes, M. R.: Does sea ice constrain the breeding schedules of high Arctic Northern Fulmars?, Condor, 109(4), 894–906, 2007.

Markovic, M. Z., VandenBoer, T. C. and Murphy, J. G.: Characterization and optimization of an online system for the simultaneous measurement of atmospheric water-soluble constituents in the gas and particle phases, J. Environ. Monit., 14(7), 1872, doi:10.1039/c2em00004k, 2012.

Martin, J., Tremblay, J.-É., Gagnon, J., Tremblay, G., Lapoussiere, A., Jose, C., Poulin, M., Gosselin, M., Gratton, Y. and Michel, C.: Prevalence, structure and properties of subsurface chlorophyll maxima in Canadian Arctic waters, Mar. Ecol.-Prog. Ser., 412, 69-84, 2010.

Martin, S. T., Hung, H.-M., Park, R. J., Jacob, D. J., Spurr, R. J. D., Chance, K. V. and Chin, M.: Effects of the physical state of tropospheric ammonium-sulfate-nitrate particles on global aerosol direct radiative forcing, Atmos. Chem. Phys., 4, 183–214, 2004.

McKane, R. B., Johnson, L. C., Shaver, G. R., Nadelhoffer, K. J., Rastetter, E. B., Fry, B., Giblin, A. E., Kielland, K., Kwiatkowski, B. L., Laundre, J. A. and Murray, G.: Resource-based niches provide a basis for plant species diversity and dominance in arctic tundra., Nature, 415, 68–71, doi:10.1038/415068a, 2002.

McKee, C. M.: Biogeochemical Cycles of Ammonia and Dimehtylsulphide in the Marine Environment, Ph.D. thesis, University of East Anglia., 2001.

McLaren, P. L.: Spring migration and habitat use by seabirds in eastern Lancaster Sound and western Baffin Bay, Arctic, 35(1), 88–111, 1982.

Monin, A. S. and Obukhov, A. M.: Basic laws of turbulent mixing in the surface layer of the atmosphere, Contrib. Geophys. Inst. Acad. Sci. USSR, 151, 163-187, 1954. (in Russian)

NASA: Fire Information Resource Management System (FIRMS), [online] Available from: https://earthdata.nasa.gov/earth-observation-data/near-real-time/firms (Accessed 30 June 2015), 2015.

Norman, M. and Leck, C.: Distribution of marine boundary layer ammonia over the Atlantic and Indian Oceans during the Aerosols99 cruise, J. Geophys. Res., 110, D16302, doi:10.1029/2005JD005866, 2005.

Paulot, F., Jacob, D. J., Johnson, M. T., Bell, T. G., Baker, A. R., Keene, W. C., Lima, I. D., Doney, S. C. and Stock, C. A.: Global oceanic emission of ammonia: Constraints from seawater and atmospheric observations, Global Biogeochem. Cycles, 29, doi:10.1002/2015GB005106, 2015.

Petters, M. D. and Kreidenweis, S. M.: A single parameter representation of hygroscopic growth and cloud condensation nucleus activity, Atmos. Chem. Phys., 7, 1961-1971, 2007.

Quinn, P. K., Charlson, R. J. and Bates, T. S.: Simultaneous observations of ammonia in the atmosphere and ocean, Nature, 335, 336–338, doi:10.1038/335336a0, 1988.

Quinn, P. K., Bates, T. S., Johnson, J. E., Covert, D. S. and Charlson, R. J.: Interactions between the sulfur and reduced nitrogen cycles over the central Pacific Ocean, J. Geophys. Res., 95, 16405–16416, 1990.

Quinn, P. K., Asher, W. E. and Charlson, R. J.: Equilibria of the Marine Muitiphase Ammonia System, J. Atmos. Chem., 14, 11–30, 1992.

Quinn, P. K., Barrett, K. J., Dentener, F. J., Lipschultz, F. and Six, K. D.: Estimation of the air/sea exchange of ammonia for the North Atlantic Basin, Biogeochemistry, 35(1), 275–304, doi:10.1007/BF02179831, 1996.

Reis, S., Pinder, R. W., Zhang, M., Lijie, G. and Sutton, M. A.: Reactive nitrogen in atmospheric emission inventories, Atmos. Chem. Phys., 9, 7657–7677, doi:10.5194/acp-9-7657-2009, 2009.

Riddick, S. N., Dragosits, U., Blackall, T. D., Daunt, F., Wanless, S. and Sutton, M. A.: The global distribution of ammonia emissions from seabird colonies, Atmos. Environ., 55, 319–327, doi:10.1016/j.atmosenv.2012.02.052, 2012.

Riddick, S. N., Dragosits, U., Blackall, T. D., Daunt, F., Wanless, S. and Sutton, M. A.: Global ammonia emissions from seabirds. NERC Environmental Information Data Centre. doi:10.5285/c9e802b3-43c8-4b36-a3a3-8861d9da8ea9, 2012b.

Riddick, S. N., Blackall, T. D., Dragosits, U., Daunt, F., Braban, C. F., Tang, Y. S., MacFarlane, W., Taylor, S., Wanless, S. and Sutton, M. A.: Measurement of ammonia emissions from tropical seabird colonies, Atmos. Environ., 89, 35–42, doi:10.1016/j.atmosenv.2014.02.012, 2014.

Schmidt, S., Mackintosh, K., Gillett, R., Pudmenzky, A., Allen, D. E., Rennenberg, H. and Mueller, J. F.: Atmospheric concentrations of ammonia and nitrogen dioxide at a tropical coral cay with high seabird density., J. Environ. Monit., 12(2), 460–465, doi:10.1039/b910922f, 2010.

Seabird Information Network: Circumpolar Seabird Data Portal, [online] Available from: http://axiom.seabirds.net/circumpolar_portal.php (Accessed 13 March 2015), 2015.

Sharma, S., Barrie, L. A., Plummer, D., Mcconnell, J. C., Brickell, P. C., Levasseur, M., Gosselin, M. and Bates, T. S.: Flux estimation of oceanic dimethyl slufide around North America, J. Geophys. Res., 104, 21327–21342, 1999.

Sharma, S., Chan, E., Ishizawa, M., Toom-Sauntry, D., Gong, S. L., Li, S.-M., Tarasick, D. W., Leaitch, W. R., Norman, A.-L., Quinn, P. K., Bates, T. S., Levasseur, M., Barrie, L. A. and Maenhaut, W.: Influence of transport and ocean ice extent on biogenic aerosol sulfur in the Arctic atmosphere, J. Geophys. Res.-Atmos., 117, D12209, doi:10.1029/2011JD017074, 2012.

Shaver, G. R. and Chapin III, F. S.: Response to fertilization by various plant growth forms in an Alaskan tundra: nutrient accumulation and growth, Ecology, 61(3), 662–675, doi:10.2307/1937432, 1980.

Skamarock, W. C., Klemp, J. B., Dudhia, J., Gill, D. O., Barker, D. M., Wang, W. and Powers, J. G.: A description of the advanced research WRF version 2, National Center for Atmospheric Research, Technical Note, 88 pp., 2005.

Stewart, K. J., Brummell, M. E., Coxson, D. S. and Siciliano, S. D.: How is nitrogen fixation in the high arctic linked to greenhouse gas emissions?, Plant Soil, 362, 215–229, doi:10.1007/s11104-012-1282-8, 2012.

Stewart, K. J., Grogan, P., Coxson, D. S. and Siciliano, S. D.: Topography as a key factor driving atmospheric nitrogen exchanges in arctic terrestrial ecosystems, Soil Biol. Biochem., 70(3), 96–112, doi:10.1016/j.soilbio.2013.12.005, 2014.

Stohl, A., Forster, C., Frank, A., Seibert, P., and Wotawa, G.: Technical note: The Lagrangian particle dispersion model FLEXPART version 6.2, Atmos. Chem. Phys., 5, 2461-2474, doi:10.5194/acp-5-2461-2005, 2005.

Sutton, M. A., Reis, S., Riddick, S. N., Dragosits, U., Nemitz, E., Theobald, M. R., Tang, Y. S., Braban, C. F., Vieno, M., Dore, A. J., Mitchell, R. F., Wanless, S., Daunt, F., Fowler, D., Blackall, T. D., Milford, C., Flechard, C. R., Loubet, B., Massad, R., Cellier, P., Personne, E., Coheur, P. F., Clarisse, L., Van Damme, M., Ngadi, Y., Clerbaux, C., Skjøth, C. A., Geels, C., Hertel, O., Wichink Kruit, R. J., Pinder, R. W., Bash, J. O., Walker, J. T., Simpson, D., Horváth, L., Misselbrook, T. H., Bleeker, A., Dentener, F. and de Vries, W.: Towards a climate-dependent paradigm of ammonia emission and deposition., Phil. Trans. R. Soc. B, 368, doi:10.1098/rstb.2013.0166, 2013.

Takahashi, T., Sutherland, S. C., Chipman, D. W., Goddard, J. G. and Ho, C.: Climatological distributions of pH, pCO_2, total CO_2, alkalinity, and $CaCO_3$ saturation in the global surface ocean, and temporal changes at selected locations, Mar. Chem., 164, 95–125, doi:10.1016/j.marchem.2014.06.004, 2014.

Tewari, M., Chen, F., Wang, W., Dudhia, J., LeMone, M. A., Mitchell, K., Ek, M., Gayno, G., Wegiel, J. and Cuenca, R. H.: Implementation and verification of the unified NOAH land surface model, 20th Conference on Weather Analysis and Forecasting/16th Conference on Numerical Weather Prediction, Seattle, WA, American Meteorolgical Society, 2004.

Theobald, M. R., Crittenden, P. D., Hunt, A. P., Tang, Y. S., Dragosits, U. and Sutton, M. A.: Ammonia emissions from a Cape fur seal colony, Cape Cross, Namibia, Geophys. Res. Lett., 33, L03812, doi:10.1029/2005GL024384, 2006.

Van Cleve, K. and Alexander, V.: Nitrogen cycling in tundra and boreal ecosystems, in Terrestrial Nitrogen Cycles, edited by F. E. Clark and T. Rosswall, pp. 375–404, Swedish National Research Council, Stockholm., 1981.

Wichink Kruit, R. J., Schaap, M., Sauter, F. J., Van Zanten, M. C. and Van Pul, W. A. J.: Modeling the distribution of ammonia across Europe including bi-directional surface-

atmosphere exchange, Biogeosciences, 9(12), 5261–5277, doi:10.5194/bg-9-5261-2012, 2012.

Wilson, L. J., Bacon, P. J., Bull, J., Dragosits, U., Blackall, T. D., Dunn, T. E., Hamer, K. C., Sutton, M. A. and Wanless, S.: Modelling the spatial distribution of ammonia emissions from seabirds in the UK, Environ. Pollut., 131(2), 173–185, doi:10.1016/j.envpol.2004.02.008, 2004.

Zhu, R., Sun, J., Liu, Y., Gong, Z. and Sun, L.: Potential ammonia emissions from penguin guano, ornithogenic soils and seal colony soils in coastal Antarctica: effects of freezing-thawing cycles and selected environmental variables, Antarct. Sci., 23, 78–92, doi:10.1017/S0954102010000623, 2011.

1 Table 1. Parameterizations and options used for the NETCARE WRF simulations

Atmospheric process	WRF option
Planetary Boundary Layer	Mellor–Yamada–Janjic Scheme (MYJ) (Janjic, 1994)
Surface layer	Monin-Obukhov Janjic Eta similarity scheme (Monin and Obukhov, 1954; Janjic, 1994, 1996, 2002)
Land surface	Unified Noah Land Surface Model (Tewari et al., 2004)*
Microphysics	WRF Single-Moment 5-class scheme (Hong, Dudhia, and Chen, 2004)
SW radiation	Goddard Shortwave Scheme (Chou and Suarez, 1994)
LW radiation	RRTMG (Iacono et al., 2008)
Cumulus parameterization	Kain–Fritsch Scheme (Kain, 2004)

2 *with corrected calculation of skin temperature over sea ice when snow melting is occurring,
3 see http://www2.mmm.ucar.edu/wrf/users/wrfv3.7/updates-3.7.1.html.
4

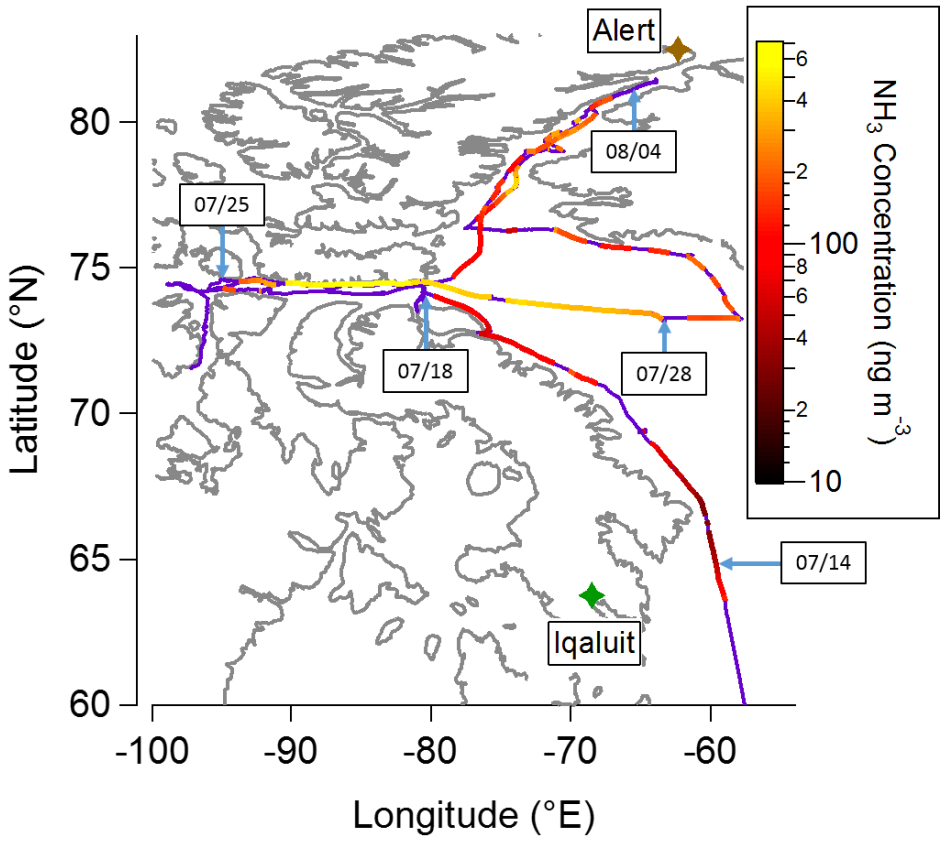

Figure 1. CCGS *Amundsen* ship track coloured by gas-phase NH_3 concentrations measured by the AIM-IC. Invalid measurements (e.g. instrument troubleshooting, influenced by ship) are purple along the ship track. Units of ng m^{-3} were chosen as a convenience for flux calculations. At STP, 100 ng $m^{-3} \approx 130$ pptv. Relevant landmarks are also labelled. Dates and arrows indicate the position of the ship at 0:00 UTC on that day.

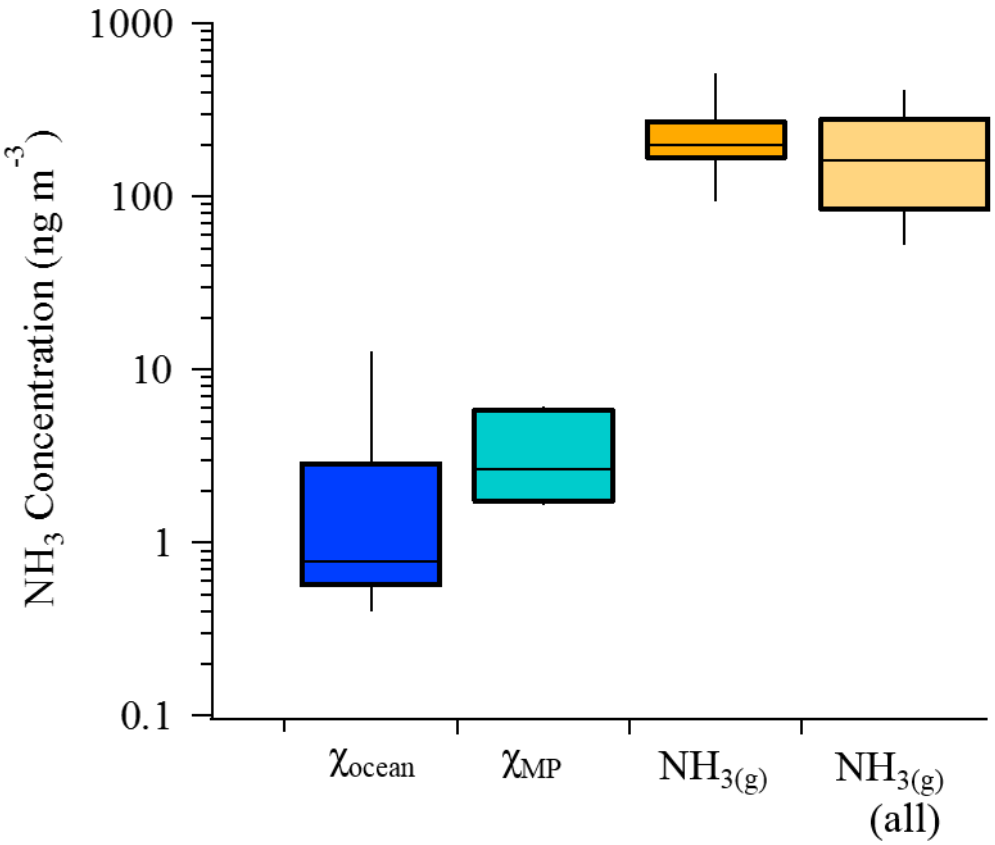

Figure 2. Box-and-whisker plot showing the observed ranges of χ (on a log scale) for both the ocean surface (dark blue) and melt ponds (light blue). The range of $NH_{3(g)}$ measured by the AIM-IC near the time of surface sampling is shown in darker yellow whereas $NH_{3(g)}$ over the entire campaign is shown in lighter yellow. The box represents 25th to 75th percentile while the line within the box denotes the median. Whiskers extend to the 10th and 90th percentile.

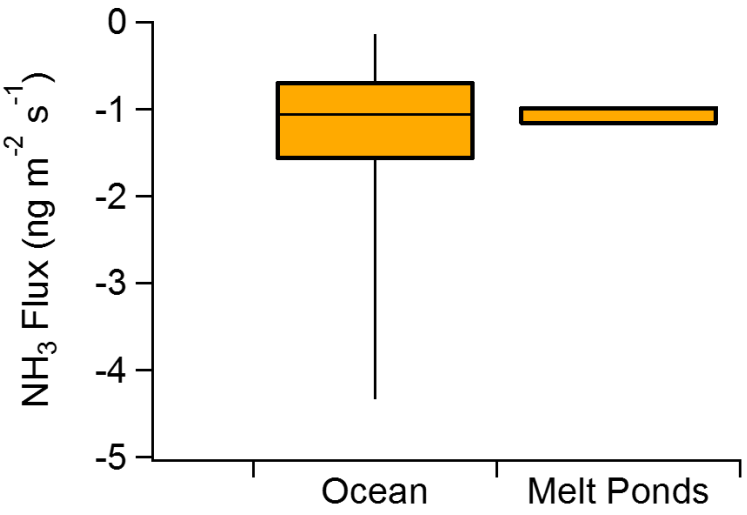

Figure 3. Box-and-whisker plot of the estimated fluxes into the open ocean and melt ponds. The percentiles are represented in the same fashion as Fig. 2.

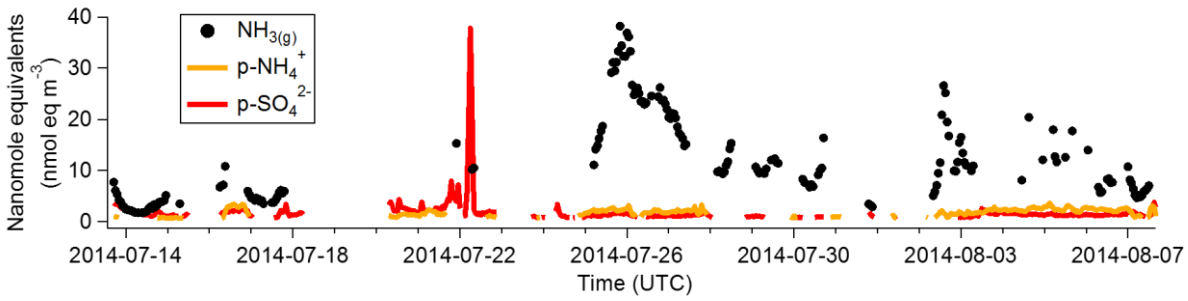

Figure 4. Time series of neq m^{-3} for $NH_{3(g)}$ (black dots), NH_4^+ in $PM_{2.5}$ (orange trace), and SO_4^{2-} in $PM_{2.5}$ (red trace). Interruptions in the data are a result of zero air experiments, calibrations, values below detection limit, instrument downtime, and (for gas-phase species) periods when the wind direction/speed were not conducive for ambient sampling (as explained in detail in section 2.2).

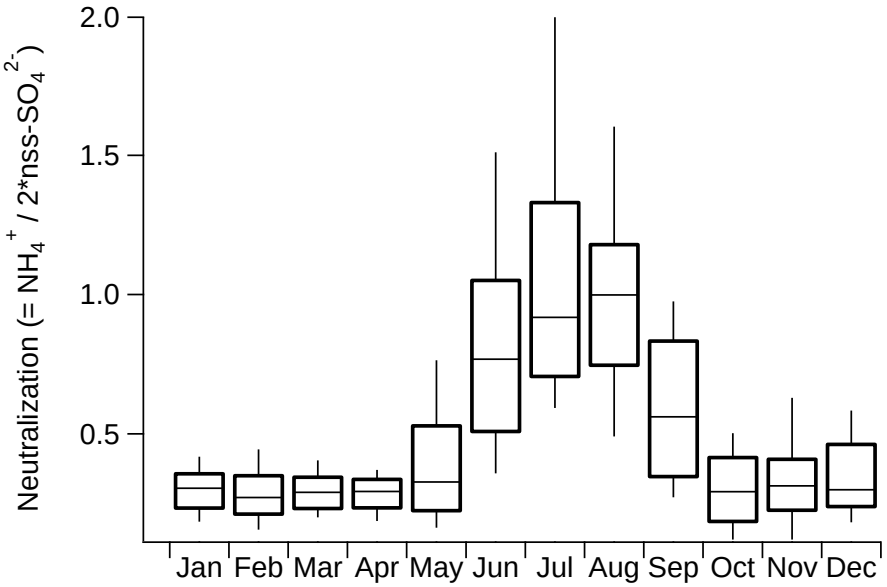

Figure 5. Box-and-whisker plot of neutralization (defined as $NH_4^+/2*nss\text{-}SO_4^{2-}$) for fifteen years (1996-2011) of weekly $PM_{2.5}$ speciation measurements taken at Alert, Nunavut. The percentiles are represented in the same fashion as Fig. 2.

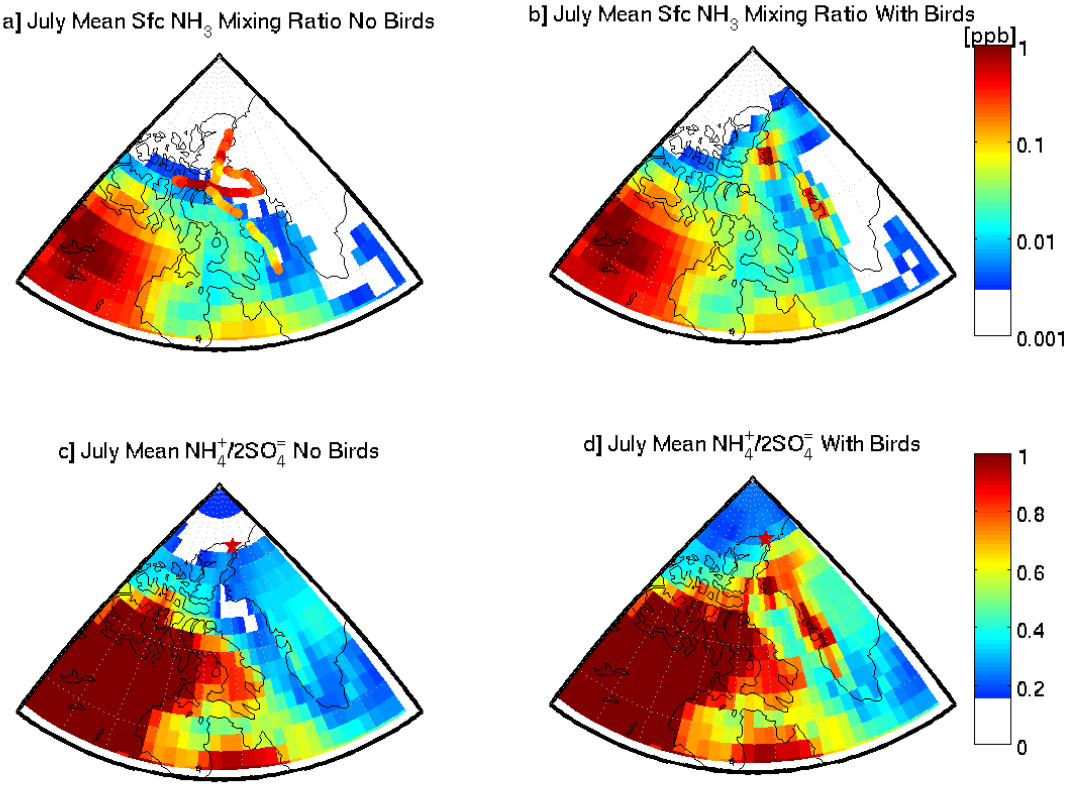

1

2 Figure 6. GEOS-Chem simulation of NH_3 mixing ratio (ppb) of the July monthly mean surface
3 layer for (a) no seabird emissions and (b) with seabird emissions. Circles in (a) represent the
4 ship track coloured by NH_3 measurements. Panels (c) and (d) show GEOS-Chem simulations
5 for the ammonium to non-sea salt sulphate ratio during the same period for (c) no seabird
6 emissions and (d) with seabird emissions. The star indicates the average ratio observed at Alert
7 during July.

8

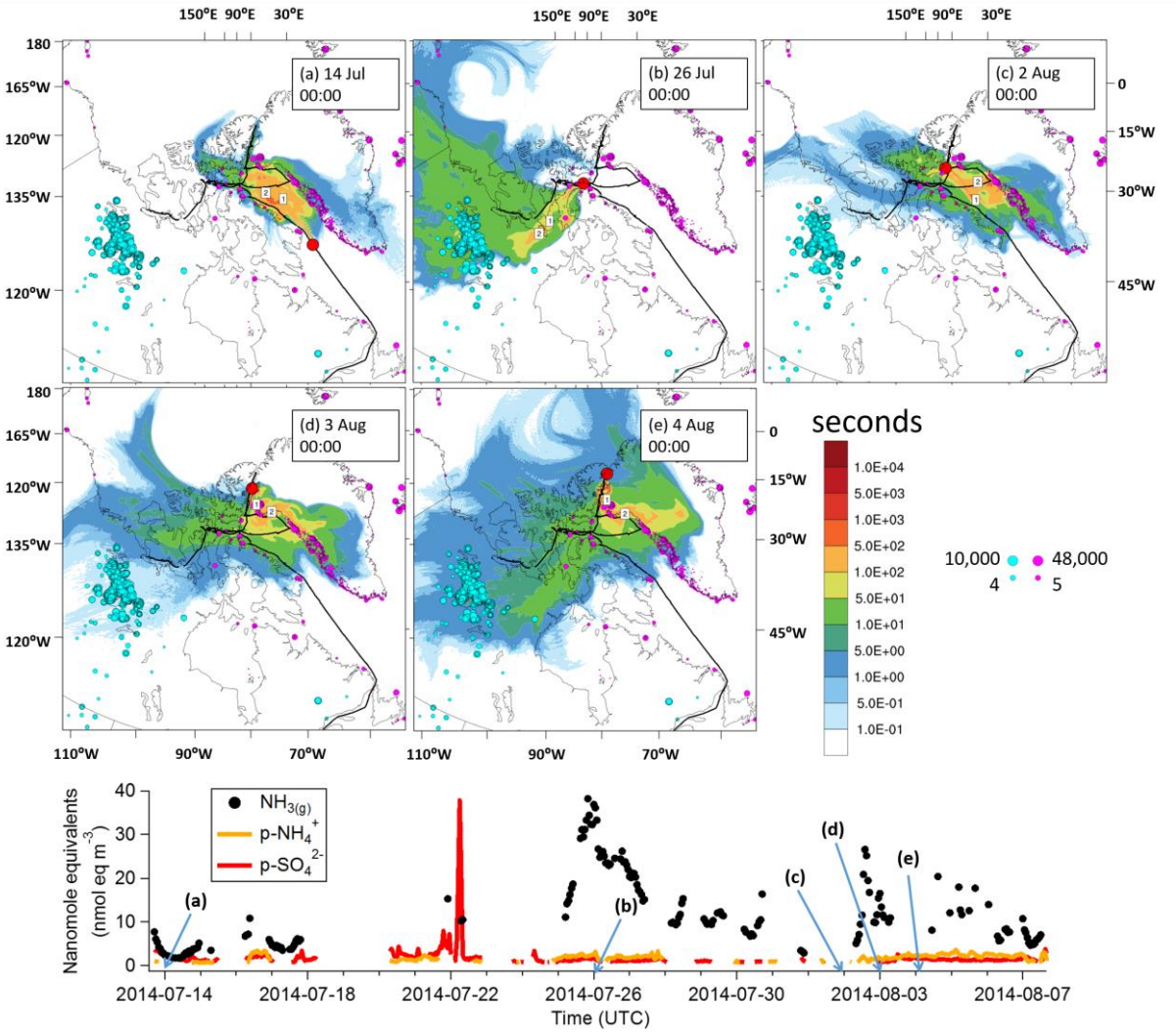

Figure 7. PES plots of FLEXPART-WRF seven day retroplumes from the ship's location on (a) 14 July 00:00, (b) 26 July 00:00, (c) 2 August 00:00, (d) 3 August 00:00 and (e) 4 August 00:00. The ship track is shown in black and the ship location at the release time is indicated in red. Colours show the airmass residence time prior to arrival at the ship (PES) in seconds. The plume centroid locations at 1 and 2 days (the approximate lifetime of NH_3) before release are shown (numbers 1 and 2). Purple circles represent the location of bird colonies with the size of each circle indicating the magnitude of estimated NH_3 emissions (in Mg NH_3 yr^{-1}). Blue circles show the location of wildfires from the NASA FIRMS measurements of fire radiative power from July 20-26 (in MW). The bottom panel is a time series of $NH_{3(g)}$ and particle-phase NH_4^+ and SO_4^{2-} measured by the AIM-IC with arrows indicating times of retroplume initiation in the upper panels. The NASA FIRMS dataset was provided by LANCE FIRMS operated by NASA/GSFC/ESDIS with funding from NASA/HQ.

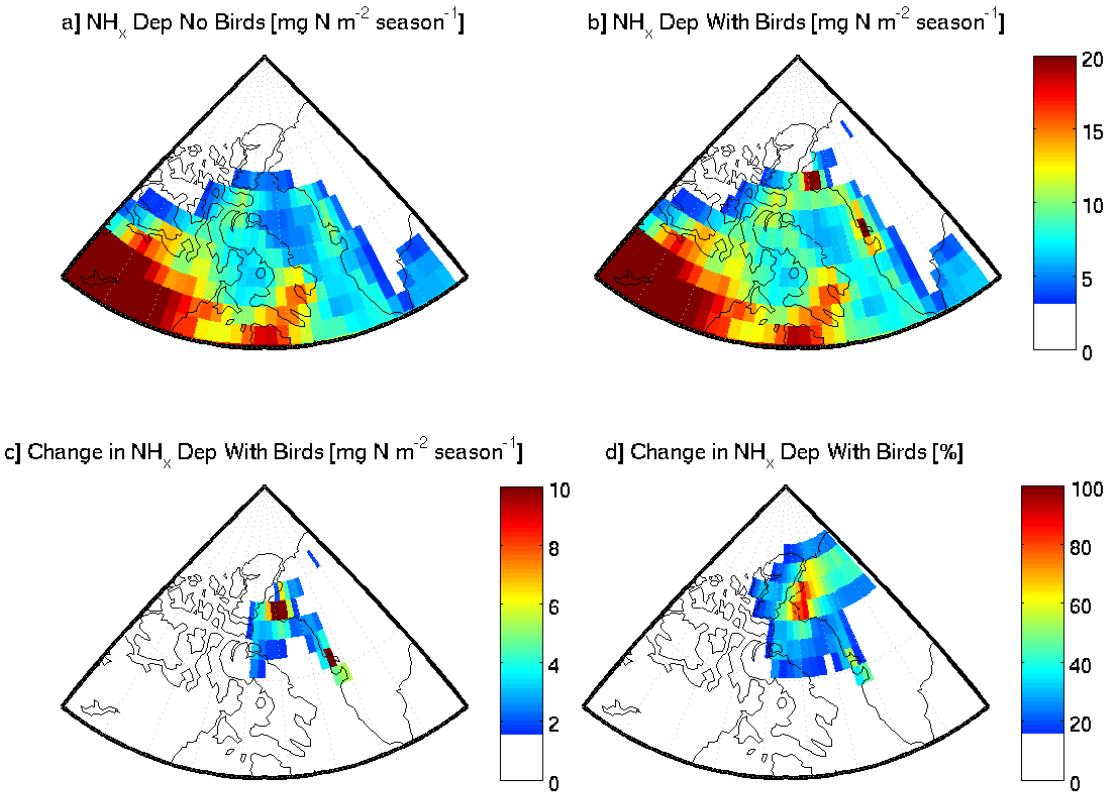

1

2 Figure 8. GEOS-Chem simulation of for total NH_x deposition (in mg N m^{-2} $season^{-1}$) for the
3 months May to September (inclusive). Panel (a) does not include seabird emissions, whereas
4 the panel (b) does. The difference in total NH_x deposition between the two emissions scenarios
5 (with birds minus without birds) is shown in panels (c) and (d) as an absolute amount and
6 percentage increase, respectively.